

Emissive Platinum(II) Cages with Reverse Fluorescence Resonance Energy Transfer for Multiple Sensing

Zeyuan Zhang,^{†,#} Zhengqing Zhao,^{†,#} Lianwei Wu,[‡] Shuai Lu,^{§,∇} Sanliang Ling,^{||} Guoping Li,[⊥] Letian Xu,[⊥] Lingzhi Ma,[†] Yali Hou,[†] Xingchen Wang,[†] Xiaopeng Li,[§] Gang He,[⊥] Kai Wang,^{*,‡} Bo Zou,[‡] Mingming Zhang^{*,†}

[†]State Key Laboratory for Mechanical Behavior of Materials, Shaanxi International Research Center for Soft Matter, School of Materials Science and Engineering, Xi'an Jiaotong University, Xi'an 710049, P. R. China


[‡]State Key Laboratory of Superhard Materials, College of Physics, Jilin University, Changchun 130012, P. R. China

[§]Department of Chemistry, University of South Florida, Tampa, Florida 33620, United States

[∇]College of Chemistry, Zhengzhou University, Zhengzhou, Henan 450001, P. R. China

^{||}Advanced Materials Research Group, Faculty of Engineering, University of Nottingham, Nottingham, NG7 2RD, United Kingdom

[⊥]Frontier Institute of Science and Technology, Xi'an Jiaotong University, Xi'an 710049, P. R. China

 Supporting Information

■ ABSTRACT

It is quite challenging to realize fluorescence resonance energy transfer (FRET) between two chromophores with specific positions and directions. Herein, through the self-assembly of two carefully selected fluorescent ligands via metal-coordination interactions, we prepared two tetragonal prismatic platinum(II) cages with reverse FRET process between their faces and pillars. Bearing different responses to external stimuli, these two emissive ligands are able to tune the FRET process, and thus making the cages sensitive to solvents, pressure and temperature. First, these cages could distinguish structurally similar alcohols such as *n*-butanol, *t*-butanol and *i*-

butanol. Furthermore, they showed decreased emission with bathochromic shifts upon high pressure. Finally, they exhibited remarkable ratiometric response to the temperature in a wide range (223~353 K) with high sensitivity. For example, by plotting the ratio of the maximum emission (I_{600}/I_{480}) of metallacage **4b** against the temperature, the slope reaches 0.072, which is among the highest values for ratiometric fluorescent thermometers reported so far. This work not only offers a strategy to manipulate the FRET efficiency in emissive supramolecular coordination complexes, but also paves the way for the future design and preparation of smart emissive materials with external stimuli responsiveness.

■ INTRODUCTION

Energy transfer is of vital importance within many significant processes including the combustion of matter, the generation of electricity, photosynthesis, etc. Fluorescence (or Förster) resonance energy transfer (FRET) describes the energy transfer between different chromophores through nonradiative dipole-dipole coupling.¹ A well-known FRET system is the energy transfer from carotenoids to chlorophyll in natural photosynthesis,² which is considered as the most important chemical reaction on the earth. Efficient FRET requires suitable distance between the energy donors and acceptors as well as good spectral overlap between the emission of the donors and the excitation of the acceptors.³ Compared with covalently linked systems, FRET systems formed via noncovalent interactions not only affords a convenient method to avoid the time-consuming synthesis, but also reduces the possibilities of emission changes caused by covalent functionalization.⁴ Therefore, various FRET-based supramolecular systems have been designed along with exploration in biomimicry,⁵ bioimaging,⁶ light-emitting materials,⁷ and photocatalysis⁸ during the past two decades.

Self-assemblies formed by coordination bonds, including metal–organic frameworks (MOFs)⁹ and supramolecular coordination complexes (SCCs),¹⁰ have become one of the most important themes in supramolecular materials during the past three decades. Abundant SCCs with fascinating structures¹¹ have been successfully constructed for guest encapsulation, catalysis, sensing and stabilizing reactive intermediates,¹² etc. Compared with other non-covalent interactions, metal-coordination interactions are still effective even at micromolar or even nanomolar concentrations,¹³ while for hydrogen bonding and host-guest interactions, the complexes dissociate dramatically upon dilution due to their low association constants for common systems.¹⁴ Therefore, metal-coordination interactions show great advantages to prepare effective FRET systems, especially because the study of FRET process should also be performed at the micromolar or even nanomolar concentration to reduce the influence of molecular aggregations. Some successful examples can be found in MOF-based systems¹⁵ in which two different chromophores are properly manipulated to achieve efficient FRET to mimic light-harvesting process in photosynthesis. However, the poor solubility and stability of MOFs in common solvents limit their processability for further applications. Although the preparation of SCCs offers an alternative way to solve this problem, metallacycles and metallacages with efficient FRET have rarely been reported,¹⁶ due to the difficulties in the design and synthesis of two compatible chromophores with ideal spectral overlap as well as the quenching of emission by transition metals (also known as heavy atom effect).¹⁷

In order to solve the heavy atom effect, Stang¹⁸ and others¹⁹ referred to the concept of aggregation induced emission (AIE)²⁰ raised by Tang et. al. and developed coordination induced emission. For AIE-based systems, the fluorophores emit strongly at high concentration or in the aggregation state while are nearly non-emissive in dilute solution. In most of the AIE-based fluorophores, propeller-like structures offer a pathway for molecular motion to deactivate the

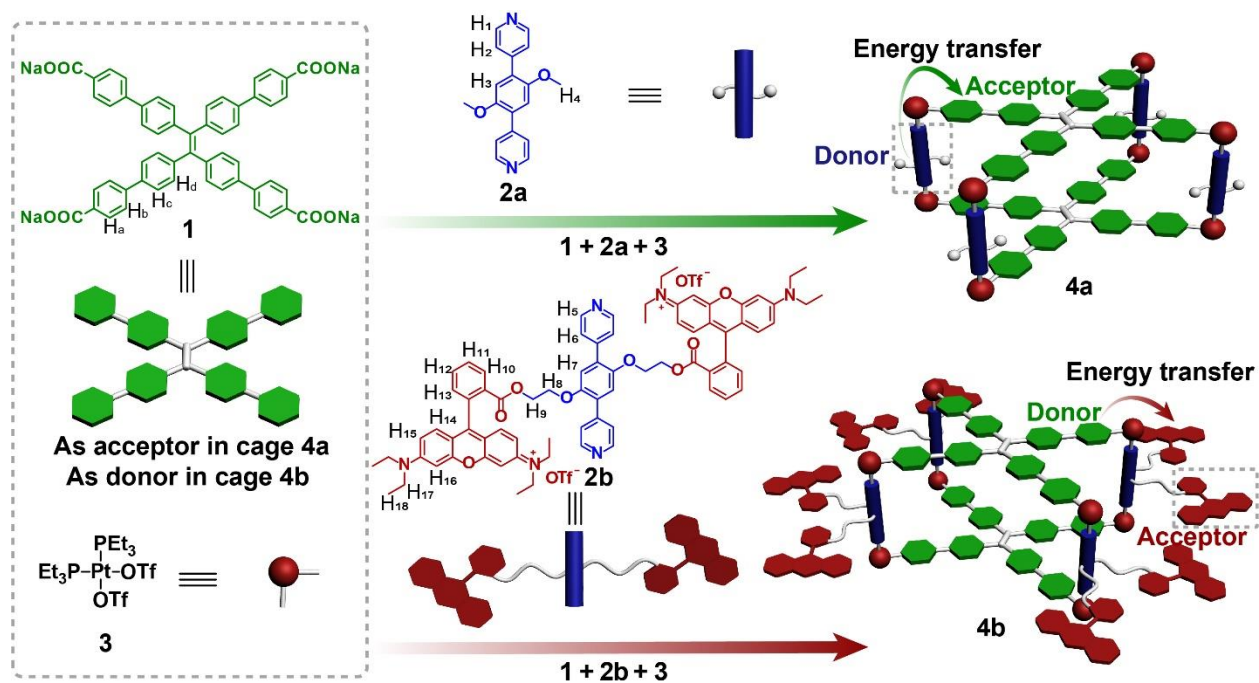
molecules in the excited state in dilute solution through thermal decay. In aggregation state, the molecular motion is restricted due to molecular aggregation, and thus reducing the non-radiative decay to give bright emission. In coordination induced emission-based systems, the motion of the molecules is restricted by coordination bonds, instead of molecular aggregation in AIE-based systems, to give strong emission. A series of emissive metallacycles and metallacages was prepared based on tetraphenylethene (TPE) for chemical sensing,²¹ light-emitting²² and light-harvesting materials.²³ However, the FRET process within these structures remains unexplored. Herein, through the careful functionalization of the pillar parts of TPE-based tetragonal prismatic platinum(II) cages,^{21b} we are able to efficiently control the FRET either from the pillars to the faces (cage **4a**) or from the faces to the pillars (cage **4b**). Moreover, because the faces (**1**) are an AIE fluorophore while the pillars (**2a** and **2b**) are aggregation caused quenching (ACQ) fluorophores²⁰ as well as their structural differences, they show different responses to temperature, mechanical pressure, and solvent composition and polarity. Such different responses further affect the spectral overlap between the energy donors and acceptors, making metallacages **4a** and **4b** very sensitive to environmental changes. Therefore, metallacages **4a** and **4b** can act as sensors for temperature, pressure and solvents. This study not only offers a convenient method to prepare SCCs with efficient energy transfer but also explores their application towards probing and sensing, which will facilitate the development of stimuli-responsive light-emitting materials.

■ RESULTS AND DISCUSSION

Design, Preparation and Characterizations of Metallacages

Based on previous study,²¹⁻²³ TPE-based benzoate ligand (**1**) which acts as the faces of the tetragonal prismatic metallacages generally absorbs in the UV region (250~400 nm) and shows a

maximum emission in the range of 480~500 nm. If TPE faces act as the acceptor within the cage, the pillar parts as the donor should emit near the UV region to achieve efficient FRET. While if TPE faces behave as the donor within the cage, the pillar parts as the acceptor should possess an obvious absorption band at ca. 480~500 nm. Moreover, the pillar molecules should be 180° dipyrindyl ligands with rigid configuration to meet the requirements for directional self-assembly. Based on these principles, we designed two metallacages with distinct FRET behaviors. First, compound **2a** with a strong emission band centered at 422 nm was chosen as the donor to prepare metallacage **4a** to study the FRET from the pillars to the faces (Scheme 1). Second, Rhodamine B, a well-known fluorophore which shows an intense absorption band from 450 nm to 600 nm and high quantum yield, was linked to the pillar parts to prepare compound **2b** as the energy acceptor to achieve efficient FRET from the faces to the pillars within metallacage **4b**. These two metallacages possess reverse FRET process either from the pillars to the faces (**4a**) or from the faces to the pillars (**4b**), which greatly influences their photophysical properties.



Scheme 1. Self-assembly of the metallacages **4a** and **4b** with reverse FRET behaviors.

The preparation of metallacages **4a** and **4b** is depicted in Scheme 1. Based on the self-assembly of TPE-based ligand **1**, dipyridyl ligands **2a** or **2b** and *cis*-Pt(PEt₃)₂(OTf)₂ **3** in a 1:2:4 molar ratio, metallacages **4a** and **4b** were synthesized in good yields (Scheme 1). The structures of metallacages **4a** and **4b** were evidenced by ³¹P{¹H} NMR and ¹H NMR spectroscopy and electrospray ionization time-of-flight mass spectroscopy (ESI-TOF MS). It can be seen from Figure 1 (spectra a-c) that the ³¹P{¹H} NMR spectra of the two metallacages split into two doublet peaks at 5.53 and 0.40 ppm for **4a**, 5.69 and 0.63 ppm for **4b**, respectively. The two peaks are of equal intensity with concomitant ¹⁹⁵Pt satellites because each platinum atom coordinates with one nitrogen atom of the pyridyl group in the pillar and one oxygen atom of the carboxylic group in the face, forming charge-separated complexes. In the ¹H NMR spectra (Figure 1, spectra f-i), the α -pyridyl protons H₁ (for **4a**) and H₅ (for **4b**) and the β -pyridyl protons H₂ (for **4a**) and H₆ (for **4b**) shifted downfield compared with their uncoordinated precursors **2a** and **2b**. It is worth noting that some protons (H₅, H₈, H₉ and H₁₇) on cage **4b** split into two set of signals because the functionalization of cages on the pillar parts reduced the symmetry of the cage, giving two different types of chemical environment for the protons. ESI-TOF gives the evidence for the coordination stoichiometry of metallacage **4a** and **4b** by showing peaks at *m/z* 1336.88 and 2304.41 (Figure 1, spectra d and e), corresponding to [M – 5OTf]⁵⁺ species of **4a** and **4b**, respectively. All these observations are consistent with previous reports,^{23a} indicating the formation of tetragonal prisms.

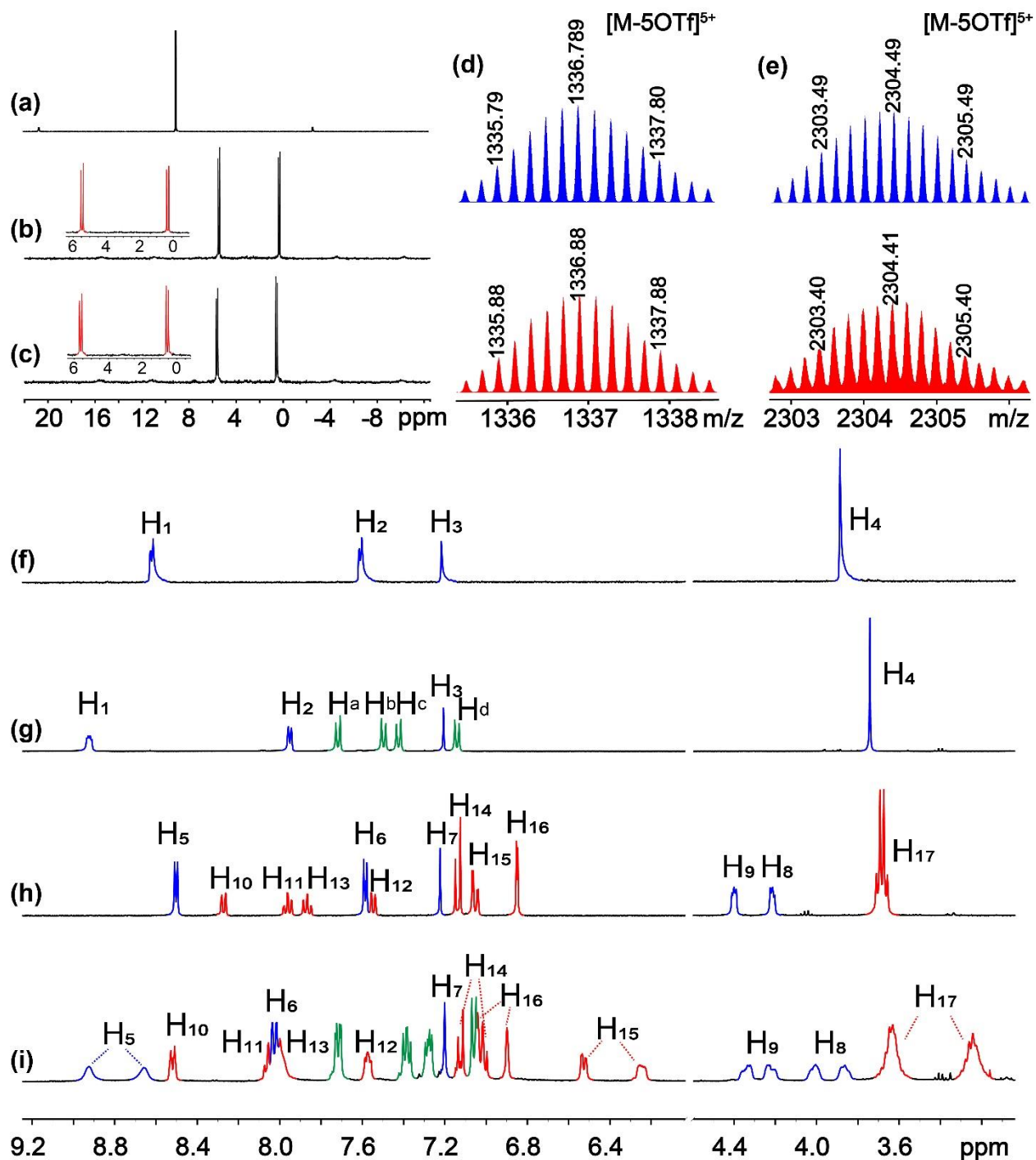


Figure 1. Partial ^{31}P { ^1H } NMR spectra (121.4 MHz, CD_3COCD_3 , 295 K) of **3** (a), **4a** (b), and **4b** (c). Experimental (red) and calculated (blue) ESI-TOF MS spectra of **4a** (d) and **4b** (e) [M – 5OTf] $^{5+}$. Partial ^1H NMR spectra (400 MHz, CD_3COCD_3 , 295 K) of **2a** (f), **4a** (g), **2b** (h), and **4b** (i). The labeling of different protons are indicated in Scheme 1.

Since all the attempts to get the crystal structures of metallacages **4a** and **4b** were unsuccessful, density functional theory (DFT) calculations (see Supporting Information for computational details) were performed in order to get insights about the structures of the metallacages **4a** and **4b** (Figure 2). The tetragonal prismatic structures were formed with TPE units as the faces, dipyriddy moieties as the pillars and 90° Pt(II) ions as the corners, respectively. The DFT optimized structure of cage **4b** shows that rhodamine groups possess two different conformations due to the steric hindrance, which causes some of the protons split into two set of peaks in the ¹H NMR spectra (Figure 1i) The DFT optimized structures of cages **4a** and **4b** reveal diameters of 4.18 nm and 5.50 nm, respectively. The TPE groups are partially rigidified and the molecular rotation of the aromatic rings are limited by the metal-coordination bonds, endowing the cages with emission properties.

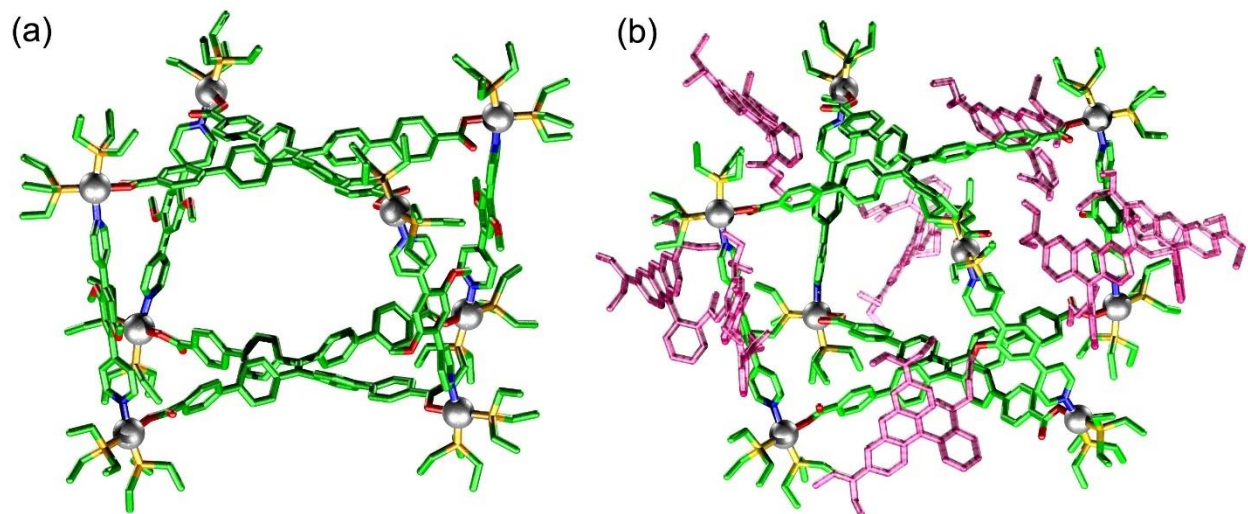


Figure 2. Optimized molecular structures of cages **4a** (a) and **4b** (b) by DFT calculations. The hydrogen atoms were omitted for clarity. Pt atoms were represented by silver balls, and the pillars and faces were represented by sticks.

Photophysical Studies

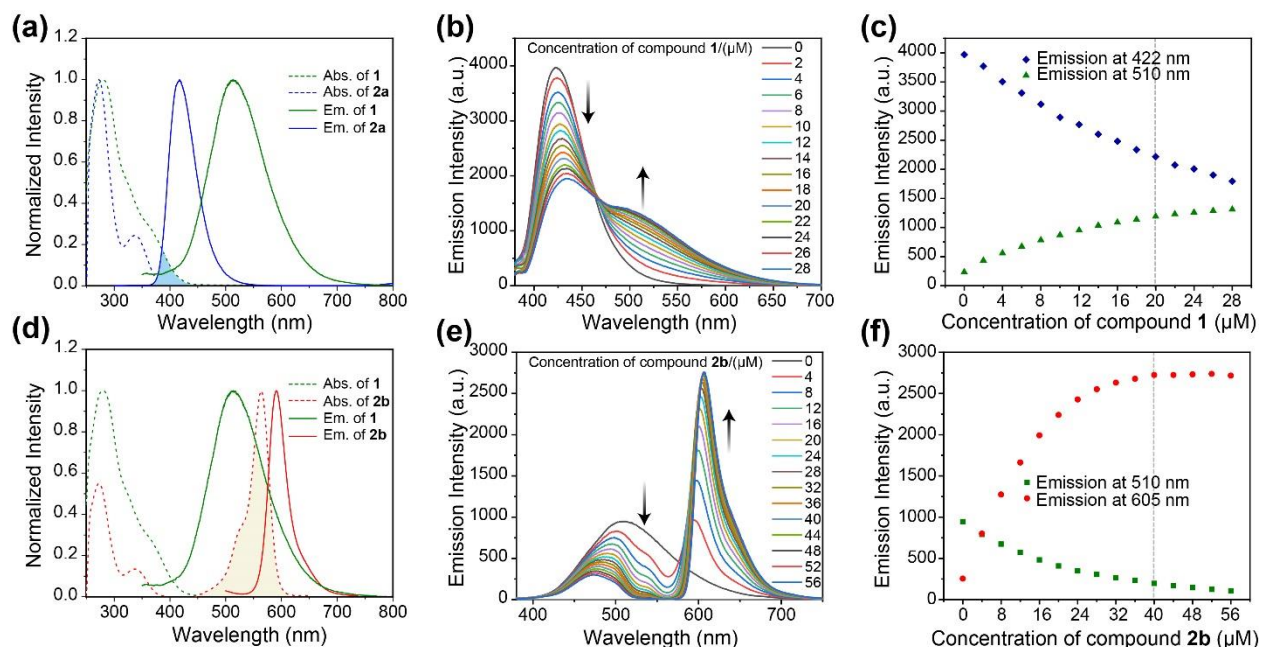


Figure 3. (a) Normalized absorption and emission spectra of the compounds **1** and **2a** in DMSO. (b) Fluorescence spectra of compound **2a** ($c = 40.0 \mu\text{M}$) and **3** ($c = 80.0 \mu\text{M}$) in a mixture of DMSO and water ($v/v = 10/1$) with different concentrations of compound **1**. (c) Fluorescent intensity changes of (b) at 422 and 510 nm. (d) Normalized absorption and emission spectra of the compounds **1** and **2b** in DMSO. (e) Fluorescence spectra of compound **1** ($c = 20.0 \mu\text{M}$) and **3** ($c = 80.0 \mu\text{M}$) in a mixture of DMSO and water ($v/v = 10/1$) with different concentrations of compound **2b**. (f) Fluorescent intensity changes of (e) at 510 and 605 nm. $\lambda_{\text{ex}} = 340 \text{ nm}$.

The photophysical properties of the individual components were first investigated to reveal their potential for FRET (See Supporting Information for details). As shown in the Figure 3a, the absorption spectrum of TPE-based ligand **1** overlaps well with the emission spectrum of compound **2a**. Similar overlap (Figure 3d) was also observed for the absorption of compound **2b** and the emission of **1**. After the formation of the metallacages, the distance between the pillars and the faces are significantly shortened (Figure 2), offering an electronic pathway to enable FRET process because of the increased dipole–dipole coupling. It can be seen clearly from the fluorescence titration experiments (Figure 3, spectra b and e) that as the gradual addition of the acceptors into

the solution of donors and *cis*-Pt(PEt₃)₂(OTf)₂ **3**, the emission of the donors decreased and that of the acceptors increased. Moreover, the fluorescence intensity remained almost unchanged when the ratios between the donors and acceptors reached their stoichiometries (Figure 3, spectra c and f). These experiments suggested the efficient energy transfer between the pillars and faces in metallacages **4a** and **4b**. Because the face molecule (TPE-based ligand **1**) is an AIE-active fluorophore and the pillar molecules (**2a** or **2b**) are ACQ fluorophores as well as their structural differences, their responses to the solvent compositions, mechanical pressure and temperature differ greatly. This makes it possible to change the degree of spectral overlap between the emission of the donors and the absorption of the acceptors under the aforementioned stimuli, thereby change the efficiency of FRET in metallacages **4a** and **4b**. Therefore, the emission of metallacages **4a** and **4b** could be very sensitive to the solvent composition, mechanical pressure and temperature, making them good candidates as chemical sensors.

Solvatochromic Properties

To understand the effect of different solvents on the photophysical properties, we first measured the UV-Vis absorption (Figure S13) and emission spectra (Figure S14) of metallacages **4a** and **4b** in several commonly used solvents. Metallacage **4a** shows an intense absorption peak centered at ca. 292 nm with a shoulder at ca. 356 nm in almost all the tested solvents; while metallacage **4b** exhibits an extra intense absorption peak at ca. 565 nm, which comes from the absorption of rhodamine moieties. However, the emission of these two cages differs a lot in different solvents (Figure S14). For example, metallacage **4a** shows only one major peak centered at 460 nm in dichloromethane while exhibits two intense emission peaks centered at ca. 412~426 nm and 462~485 nm in acetone, acetonitrile, chloroform, DMF and DMSO. Metallacage **4b** exhibits two emission peaks at around 470 nm and 605 nm in dichloromethane, chloroform, DMF, DMSO while

shows almost one peak at ca. 600 nm in acetone and acetonitrile. Factors which may contribute to the vast differences on emissions of our metallacages in different solvents may include: 1) the different emission behaviors of the faces with AIE and the pillars with ACQ; 2) the different solubilities of the metallacages in different solvents; 3) the different FRET efficiency in different solvents (Figure S16).

The sensitivity of metallacages towards different solvents inspired us to explore the use of their emission to distinguish structurally similar alcohols. The stability of the metallacages was first studied. The ^{31}P { ^1H } NMR and ^1H NMR spectra (Figures S17) of metallacage **4a** in methanol stay unchanged upon the addition of different alcohols including ethanol (EtOH), *t*-butanol (*t*-BuOH) and ethyl glycol, indicating that the cages are chemostable in common alcohols. As shown in Figure 4, the maximum emission and the intensity of the cages are different in the tested alcohols. Metallacage **4a** shows maximum emission centered at 439 nm, 440 nm and 414 nm in *n*-butanol, *i*-butanol and *t*-butanol, respectively (Figure 4a). For metallacage **4b**, the alcohols could be distinguished by the ratio of its two emission bands (Figure 4b). Both cages show different Commission internationale de l'éclairage (CIE) chromaticity coordinates in the three structural similar alcohols (Figure 4c). Among three types of BuOH, *t*-BuOH can be easily distinguished from *n/i*-BuOH by the naked eyes due to their color differences (insets of Figures 4a and 4b). With the help of CIE chromaticity coordinates, the three types of alcohols can be readily distinguished. We note the emission energy of **4a** in *t*-BuOH is different from that in *n/i*-BuOH, perhaps due to different solvent polarity (Table S3). On the other hand, the emission energies of **4b** in different solvents are the same, which may be associated with the different characteristics of the lowest excited states of **4a** and **4b** (Figure S22). Furthermore, the different emission intensities of **4a** and **4b** in different solvents could be attributed to the different solvent viscosities (Table S3); more

viscous solvent (e.g. *t*-BuOH) tends to show higher emission intensity, due to suppressed collisions between fluorescent molecules with less energy lost (as heat) through non-radiative decay.

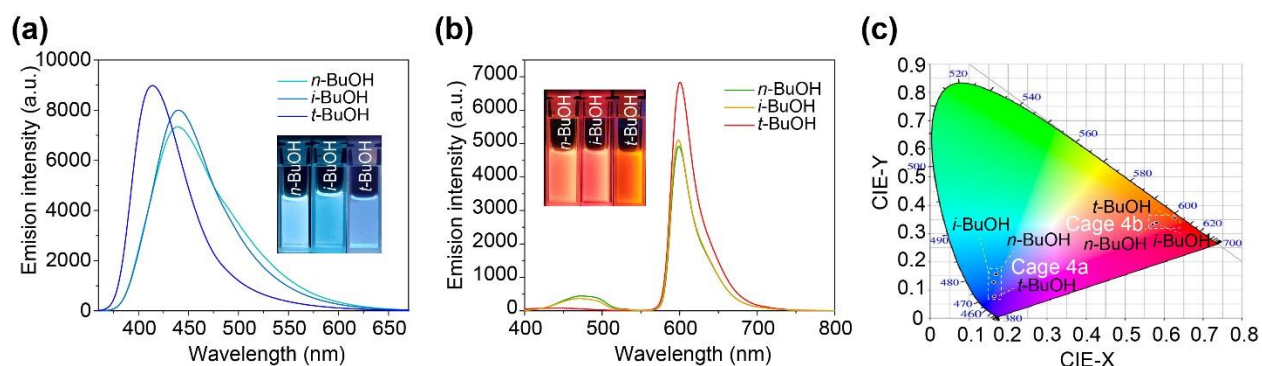


Figure 4. Fluorescence spectra of (a) cage **4a** and (b) cage **4b** and (c) their corresponding CIE chromaticity coordinates in different alcohols ($\lambda_{\text{ex}} = 340 \text{ nm}$, $c = 10.0 \mu\text{M}$). Insets: photographs of cages **4a** and **4b** upon the excitation at 365 nm using a UV lamp at 298 K.

Mechanochromic Properties

Mechanochromic materials which change their emission in response to external forces have been widely used in fluorescent switches and devices.²⁴ Although the piezofluorochromic properties of TPE-based small molecules²⁵ and MOFs²⁶ have been intensively studied, the mechanochromic response of TPE-based metallacages has been rarely addressed. In order to study the structural response under high pressure, the fluorescence upon stress was collected *in situ* by diamond anvil cell technique.²⁷ Metallacages **4a** and **4b** show light-green and deep-red emission with maximum emission at ca. 500 nm and 605 nm, respectively, under ambient conditions. Upon compression, the photoluminescence maximum of metallacages **4a** and **4b** experienced large bathochromic shift to 620 nm at 14.1 GPa, and 700 nm at 12.1 GPa, respectively. Moreover, the emission intensity decreased significantly as the pressure increased and the whole process was fully reversible at least for 10 cycles (Figure S52). We speculate that the mechanochromic response of our metallacages is because of more tightly molecular packing due to the mechanical compression, and as a result, the pillars become tilted and the TPE faces become more planarized,

which affect the dipole–dipole coupling between the pillars and the faces and therefore the emission wavelength and intensity. We note similar mechanochromic response was also observed in TPE-containing MOF-based systems²⁶ and AIE-fluorophore-based cocrystals.²⁸

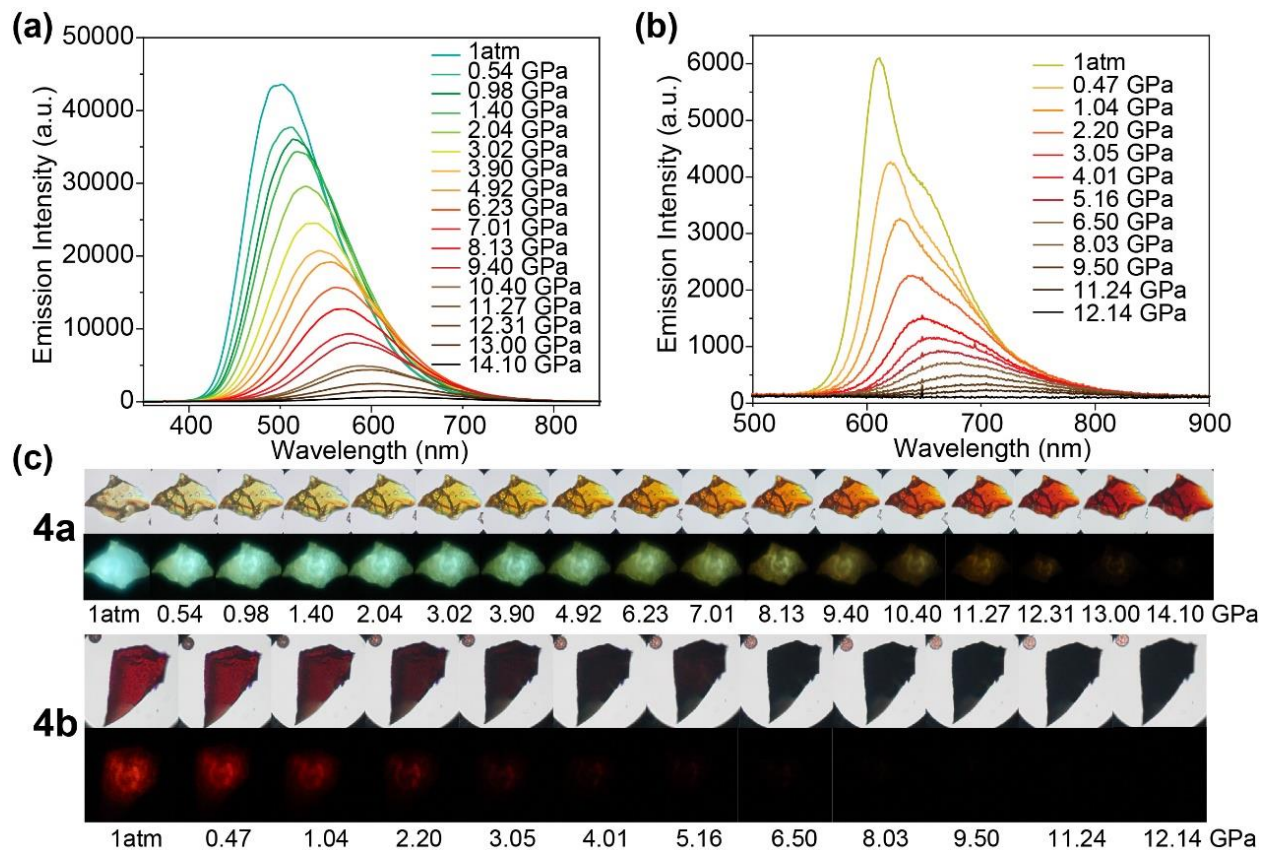


Figure 5. Emission spectra of cages **4a** (a) and **4b** (b) under different pressures and their optical and fluorescence images (c).

Thermochromic Property

Temperature-responsive luminescent materials with two different emission bands can act as ratiometric fluorescent thermometers to improve the accuracy and precision via self-calibration.²⁹ In metallacages **4a** and **4b**, two fluorophores which may display different response to the temperature were incorporated and the temperature change were expected to influence the efficiency of FRET. This motivated us to further study their response towards temperature changes. DMF was chosen as the solvent because it can be used in a wide range of temperature

based on its low freezing point (-61 °C) and high boiling point (153 °C). The NMR spectra recorded for cages **4a** and **4b** in DMF-*d*₇ are similar with the spectra in acetone-*d*₆, indicating that they are chemostable in DMF (Figures S53-S61). As shown in Figures 6a, as the temperature increased, the emission at 425 nm corresponding to the donor increased, while the emission at 488 nm that ascribed to the acceptor decreased for metallacage **4a** upon the excitation at 340 nm. A linear fitting curve (slope = -0.006) of I_{488}/I_{425} versus temperature (Figure 6c) was plotted, indicating that metallacage **4a** may serve as a fluorescent thermometer in the range from 223 K to 353 K. Similar with metallacage **4a**, increased donor emission at 480 nm and decreased acceptor emission at 600 nm were observed for **4b** as the increase of the temperature. The ratio of the maximum emission (I_{600}/I_{480}) also decreased linearly with the temperature in the range from 233 K to 333 K. Remarkably, the absolute value of slope is 0.072, which is among the highest values for ratiometric fluorescent thermometers reported so far.²⁹ This indicates that the increase of temperature can decrease the efficiency of FRET, perhaps due to the partially dissociation of the metal-coordination bonds at high temperature.

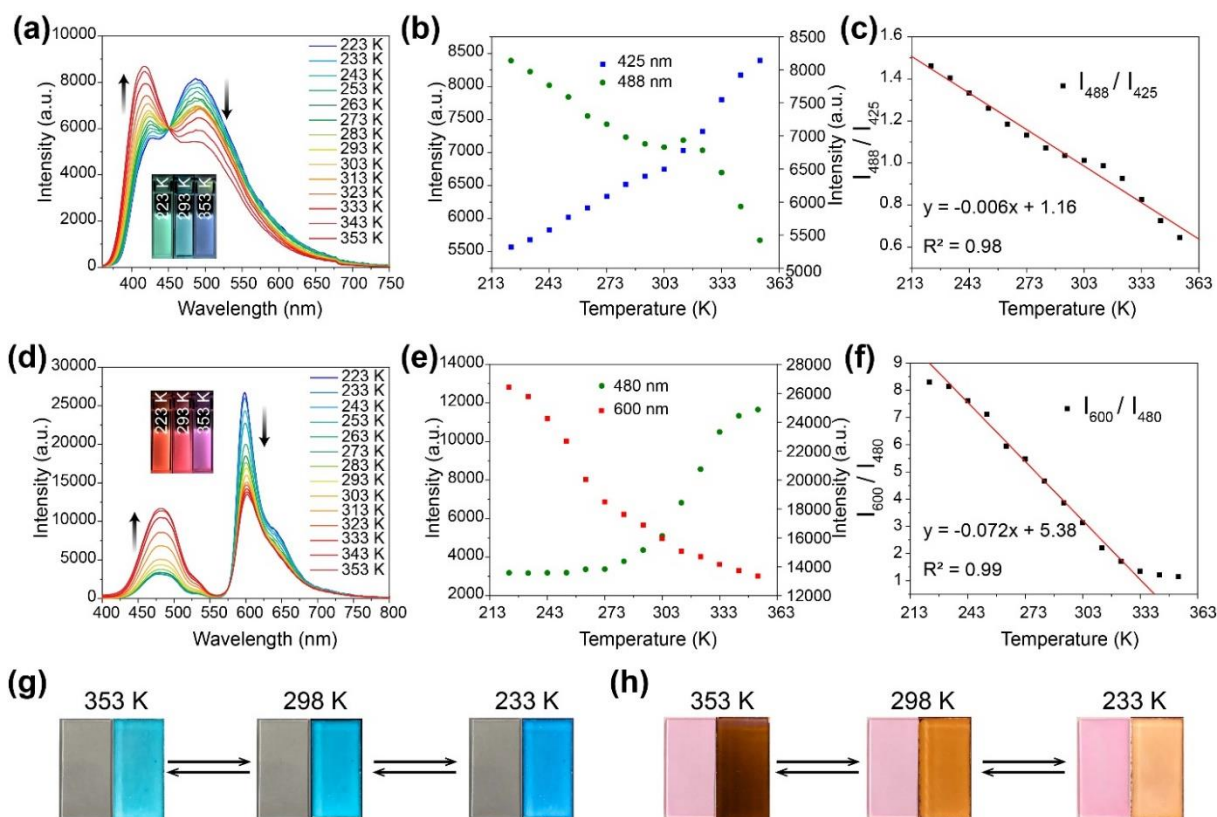


Figure 6. (a) Fluorescence spectra of cage **4a** ($c = 10.0 \mu\text{M}$) in DMF at different temperature. (b) fluorescent intensity changes of cage **4a** at 425 and 488 nm. (c) Plots of the I_{488}/I_{425} versus temperature. (d) fluorescence spectra of cage **4b** ($c = 10.0 \mu\text{M}$) in DMF at different temperature. (e) fluorescent intensity changes of cage **4b** at 480 and 600 nm. (f) Plots of the I_{600}/I_{480} versus temperature. Optical and fluorescent photographs of **4a** (g) and **4b** (h) at different temperature.

Encouraged by the fluorescence changes of the metallacages along with temperature in solution,³⁰ two thin films were prepared by doping the metallacages into polyvinylidene fluoride (PVDF). Although no obvious color changes were observed from the optical photographs of the films at different temperature, their fluorescent photographs differ dramatically at different temperature (Figures 6g and 6h). The whole process is fully reversible after 10 cycles, indicating that the metallacages can serve as good sensor for temperature. Different from most fluorescent thermometers that are prepared solely based on the intensity changes, our system offers an

approach to manipulate two fluorophores with efficient FRET in a single supramolecular system to prepare ratiometric thermometers, which will pave the way for the further design of fluorescent thermometers.

■ CONCLUSION

In summary, two tetragonal prismatic platinum(II) cages with reverse energy transfer between their pillars and faces were prepared and characterized by ^{31}P NMR and ^1H NMR spectroscopy, ESI-TOF-MS, UV absorption, and fluorescence spectroscopy. Because of their different fluorescent properties of the two ligands, they show different response to external stimuli including solvent polarity, composition, pressure and temperature, which significantly change the efficiency of FRET, thus influencing the emission of the cages. Their use to distinguish structural similar alcohols and as fluorescent ratiometric thermometers were explored, showing their potential applications as highly sensitive chemical sensors. This study not only provides a type of metal-coordinated structures in which the efficiency of FRET can be finely tuned between their building blocks, but also takes advantage of such response to explore their practical application for chemical and temperature sensing. As such it will open a new avenue for stimuli-responsive and light-emitting materials, sensors and bioimaging.

■ ASSOCIATED CONTENT

Supporting Information

The supporting information is available free of charge via the Internet at <http://pubs.acs.org>. Syntheses and characterization data (NMR, Fluorescence Spectra), including Figures S1–S42.

■ AUTHOR INFORMATION

Corresponding Author

mingming.zhang@xjtu.edu.cn; kaiwang@jlu.edu.cn

Author Contributions

#Z. Z. and Z. Z. contributed equally to this work.

Notes

The authors declare no competing financial interest.

■ ACKNOWLEDGMENTS

This work was supported by the National Natural Science Foundation of China (21801203 to M. Z., 11774120 to K. W., 21725304 to B. Z.), National Institutes of Health (R01GM128037 to X. L.), and The Key Research and Development Program of Shaanxi Province (2019KW-019 to M.Z.). M. Z. is thankful for start-up funds from Xi'an Jiaotong University. We thank Dr. Gang Chang and Yu Wang at Instrument Analysis Center and Dr. Aquan Zheng and Junjie Zhang at Experimental Chemistry Center of Xi'an Jiaotong University for NMR and fluorescence measurements.

■ REFERENCES

- (1) (a) Förster, T. Zwischenmolekulare Energiewanderung und Fluoreszenz. *Ann. Phys.* **1948**, 437, 55-75. (b) Förster, T. Transfer Mechanisms of Electronic Excitation. *Discuss. Faraday Soc.* **1959**, 27, 7-17.
- (2) Mirkovic, T.; Ostroumov, E. E.; Anna, J. M.; van Grondelle, R.; Govindjee; Scholes, G. D. Light Absorption and Energy Transfer in the Antenna Complexes of Photosynthetic Organisms. *Chem. Rev.* **2017**, 117, 249-293.
- (3) Peng, H.-Q.; Niu, L.-Y.; Chen, Y.-Z.; Wu, L.-Z.; Tung, C.-H.; Yang, Q.-Z. Biological

- Applications of Supramolecular Assemblies Designed for Excitation Energy Transfer. *Chem. Rev.* **2015**, *115*, 7502-7542.
- (4) Teunissen, A. J. P.; Perez-Medina, C.; Meijerink, A.; Mulder, W. J. M. Investigating Supramolecular Systems Using Förster Resonance Energy Transfer. *Chem. Soc. Rev.* **2018**, *47*, 7027-7044.
- (5) (a) Peng, H.-Q.; Chen, Y.-Z.; Zhao, Y.; Yang, Q.-Z.; Wu, L.-Z.; Tung, C.-H.; Zhang, L.-P.; Tong, Q.-X. Artificial Light-Harvesting System Based on Multifunctional Surface-Cross-Linked Micelles. *Angew. Chem. Int. Ed.* **2012**, *51*, 2088-2092. (b) Xu, Z.; Peng, S.; Wang, Y.-Y.; Zhang, J.-K.; Lazar, A. I.; Guo, D.-S. Broad-Spectrum Tunable Photoluminescent Nanomaterials Constructed from a Modular Light-Harvesting Platform Based on Macrocyclic Amphiphiles. *Adv. Mater.* **2016**, *28*, 7666-7671. (c) Chen, P.-Z.; Weng, Y.-X.; Niu, L.-Y.; Chen, Y.-Z.; Wu, L.-Z.; Tung, C.-H.; Yang, Q.-Z., Light-Harvesting Systems Based on Organic Nanocrystals to Mimic Chlorosomes. *Angew. Chem. Int. Ed.* **2016**, *55*, 2759-2763. (d) Guo, S.; Song, Y.; He, Y.; Hu, X.-Y.; Wang, L., Highly Efficient Artificial Light-Harvesting Systems Constructed in Aqueous Solution Based on Supramolecular Self-Assembly. *Angew. Chem. Int. Ed.* **2018**, *57*, 3163-3167.
- (6) (a) Mu, J.; Liu, F.; Rajab, M. S.; Shi, M.; Li, S.; Goh, C.; Lu, L.; Xu, Q.-H.; Liu, B.; Ng, L. G.; Xing, B. A Small-Molecule FRET Reporter for the Real-Time Visualization of Cell-Surface Proteolytic Enzyme Functions. *Angew. Chem. Int. Ed.* **2014**, *53*, 14357-14362. (b) Jia, X.; Chen, Q.; Yang, Y.; Tang, Y.; Wang, R.; Xu, Y.; Zhu, W.; Qian, X. FRET-Based Mito-Specific Fluorescent Probe for Ratiometric Detection and Imaging of Endogenous Peroxynitrite: Dyad of Cy3 and Cy5. *J. Am. Chem. Soc.* **2016**, *138*, 10778-10781. (c) Tian, M.; Ma, Y.; Lin, W. Fluorescent Probes for the Visualization of Cell Viability. *Acc. Chem. Res.* **2019**, *52*, 2147-2157.

- (7) (a) Abbel, R.; Grenier, C.; Pouderoijen, M. J.; Stouwdam, J. W.; Leclère, P. E. L. G.; Sijbesma, R. P.; Meijer, E. W.; Schenning, A. P. H. J. White-Light Emitting Hydrogen-Bonded Supramolecular Copolymers Based on π -Conjugated Oligomers. *J. Am. Chem. Soc.* **2009**, *131*, 833-843. (b) Vijayakumar, C.; Praveen, V. K.; Ajayaghosh, A. RGB Emission through Controlled Donor Self-Assembly and Modulation of Excitation Energy Transfer: A Novel Strategy to White-Light-Emitting Organogels. *Adv. Mater.* **2009**, *21*, 2059-2063. (c) Praveen, V. K.; Ranjith, C.; Armaroli, N. White-Light-Emitting Supramolecular Gels. *Angew. Chem. Int. Ed.* **2014**, *53*, 365-368.
- (8) (a) Wang, F.; Wang, W.-G.; Wang, H.-Y.; Si, G.; Tung, C.-H.; Wu, L.-Z., Artificial Photosynthetic Systems Based on FeFe-Hydrogenase Mimics: The Road to High Efficiency for Light-Driven Hydrogen Evolution. *ACS Catal.* **2012**, *2*, 407-416. (b) Hao, M.; Sun, G.; Zuo, M.; Xu, Z.; Chen, Y.; Hu, X.-Y.; Wang, L. A Supramolecular Artificial Light-harvesting System with Two-step Sequential Energy Transfer for Photochemical Catalysis. *Angew. Chem. Int. Ed.* **2019**, *58*, doi: 10.1002/anie.201912654.
- (9) (a) Horike, S.; Shimomura, S.; Kitagawa, S., Soft Porous Crystals. *Nat. Chem.* **2009**, *1*, 695-704. (b) Zhou, H.-C.; Long, J. R.; Yaghi, O. M. Introduction to Metal–Organic Frameworks. *Chem. Rev.* **2012**, *112*, 673-674. (c) Furukawa, H.; Cordova, K. E.; O’Keeffe, M.; Yaghi, O. M. The Chemistry and Applications of Metal-Organic Frameworks. *Science* **2013**, *341*, 974-986.
- (10) (a) Cook, T. R.; Zheng, Y.-R.; Stang, P. J. Metal–Organic Frameworks and Self-Assembled Supramolecular Coordination Complexes: Comparing and Contrasting the Design, Synthesis, and Functionality of Metal–Organic Materials. *Chem. Rev.* **2013**, *113*, 734-777. (b) Brown, C. J.; Toste, F. D.; Bergman, R. G.; Raymond, K. N. Supramolecular Catalysis in Metal–Ligand Cluster Hosts. *Chem. Rev.* **2015**, *115*, 3012-3035. (c) Cook, T. R.; Stang,

- P. J. Recent Developments in the Preparation and Chemistry of Metallacycles and Metallacages via Coordination. *Chem. Rev.* **2015**, *115*, 7001-7045. (d) Wang, W.; Wang, Y.-X.; Yang, H.-B. Supramolecular Transformations within Discrete Coordination-Driven Supramolecular Architectures. *Chem. Soc. Rev.* **2016**, *45*, 2656-2693. (e) Fielden, S. D. P.; Leigh, D. A.; Woltering, S. L. Molecular Knots. *Angew. Chem. Int. Ed.* **2017**, *56*, 11166-11194. (f) Chakraborty, S.; Newkome, G. R. Terpyridine-Based Metallosupramolecular Constructs: Tailored Monomers to Precise 2D-Motifs and 3D-Metallocages. *Chem. Soc. Rev.* **2018**, *47*, 3991-4016. (g) Zhang, D.; Ronson, T. K.; Nitschke, J. R. Functional Capsules via Subcomponent Self-Assembly. *Acc. Chem. Res.* **2018**, *51*, 2423-2436. (h) Jing, X.; He, C.; Zhao, L.; Duan, C., Photochemical Properties of Host–Guest Supramolecular Systems with Structurally Confined Metal–Organic Capsules. *Acc. Chem. Res.* **2019**, *52*, 100-109. (i) Sepehrpour, H.; Fu, W.; Sun, Y.; Stang, P. J. Biomedically Relevant Self-Assembled Metallacycles and Metallacages. *J. Am. Chem. Soc.* **2019**, *141*, 14005-14020.
- (11) (a) Xie, T. Z.; Guo, K.; Guo, Z.; Gao, W. Y.; Wojtas, L.; Ning, G. H.; Huang, M.; Lu, X.; Li, J. Y.; Liao, S. Y.; Chen, Y. S.; Moorefield, C. N.; Saunders, M. J.; Cheng, S. Z.; Wesdemiotis, C.; Newkome, G. R. Precise Molecular Fission and Fusion: Quantitative Self-Assembly and Chemistry of a Metallo-Cuboctahedron. *Angew. Chem. Int. Ed.* **2015**, *54*, 9224-9229. (b) Fujita, D.; Ueda, Y.; Sato, S.; Mizuno, N.; Kumasaka, T.; Fujita, M. Self-Assembly of Tetravalent Goldberg Polyhedra from 144 Small Components. *Nature* **2016**, *540*, 563-566. (c) Danon, J. J.; Kruger, A.; Leigh, D. A.; Lemonnier, J. F.; Stephens, A. J.; Vitorica-Yrezabal, I. J.; Woltering, S. L. Braiding a molecular knot with eight crossings. *Science* **2017**, *355*, 159-162. (d) Wang, H.; Liu, C. H.; Wang, K.; Wang, M.; Yu, H.; Kandapal, S.; Brzozowski, R.; Xu, B.; Wang, M.; Lu, S.; Hao, X. Q.; Eswara, P.;

- Nieh, M. P.; Cai, J.; Li, X. *J. Am. Chem. Soc.* **2019**, *141*, 16108-16116.
- (12) (a) Kishi, N.; Li, Z.; Yoza, K.; Akita, M.; Yoshizawa, M. An M_2L_4 Molecular Capsule with an Anthracene Shell: Encapsulation of Large Guests up to 1 nm. *J. Am. Chem. Soc.* **2011**, *133*, 11438-11441; (b) Li, K.; Zhang, L.-Y.; Yan, C.; Wei, S.-C.; Pan, M.; Zhang, L.; Su, C.-Y. Stepwise Assembly of $Pd_6(RuL_3)_8$ Nanoscale Rhombododecahedral Metal–Organic Cages via Metalloligand Strategy for Guest Trapping and Protection. *J. Am. Chem. Soc.* **2014**, *136*, 4456-4459. (c) Cullen, W.; Misuraca, M. C.; Hunter, C. A.; Williams, N. H.; Ward, M. D., Highly Efficient Catalysis of the Kemp Elimination in the Cavity of a Cubic Coordination Cage. *Nat. Chem.* **2016**, *8*, 231-236. (d) Cai, L.-X.; Li, S.-C.; Yan, D.-N.; Zhou, L.-P.; Guo, F.; Sun, Q.-F., Water-Soluble Redox-Active Cage Hosting Polyoxometalates for Selective Desulfurization Catalysis. *J. Am. Chem. Soc.* **2018**, *140*, 4869-4876. (e) Howlader, P.; Mondal, B.; Purba, P. C.; Zangrando, E.; Mukherjee, P. S. Self-Assembled Pd(II) Barrels as Containers for Transient Merocyanine Form and Reverse Thermochromism of Spiropyran. *J. Am. Chem. Soc.* **2018**, *140*, 7952-7960.
- (13) Chakrabarty, R.; Mukherjee, P. S.; Stang, P. J. Supramolecular Coordination: Self-Assembly of Finite Two- and Three-Dimensional Ensembles. *Chem. Rev.* **2011**, *111*, 6810-6918.
- (14) (a) De Greef, T. F. A.; Smulders, M. M. J.; Wolfs, M.; Schenning, A. P. H. J.; Sijbesma, R. P.; Meijer, E. W. Supramolecular Polymerization. *Chem. Rev.* **2009**, *109*, 5687-5754. (b) Yang, L.; Tan, X.; Wang, Z.; Zhang, X. Supramolecular Polymers: Historical Development, Preparation, Characterization, and Functions. *Chem. Rev.* **2015**, *115*, 7196-7239. (c) Yu, G.; Jie, K.; Huang, F. Supramolecular Amphiphiles Based on Host-Guest Molecular Recognition Motifs. *Chem. Rev.* **2015**, *115*, 7240-7303.
- (15) (a) Lee, C. Y.; Farha, O. K.; Hong, B. J.; Sarjeant, A. A.; Nguyen, S. T.; Hupp, J. T. Light-

- Harvesting Metal–Organic Frameworks (MOFs): Efficient Strut-to-Strut Energy Transfer in Bodipy and Porphyrin-Based MOFs. *J. Am. Chem. Soc.* **2011**, *133*, 15858-15861. (b) Kent, C. A.; Liu, D.; Ma, L.; Papanikolas, J. M.; Meyer, T. J.; Lin, W., Light Harvesting in Microscale Metal–Organic Frameworks by Energy Migration and Interfacial Electron Transfer Quenching. *J. Am. Chem. Soc.* **2011**, *133*, 12940-12943. (c) Son, H.-J.; Jin, S.; Patwardhan, S.; Wezenberg, S. J.; Jeong, N. C.; So, M.; Wilmer, C. E.; Sarjeant, A. A.; Schatz, G. C.; Snurr, R. Q.; Farha, O. K.; Wiederrecht, G. P.; Hupp, J. T., Light-Harvesting and Ultrafast Energy Migration in Porphyrin-Based Metal–Organic Frameworks. *J. Am. Chem. Soc.* **2013**, *135*, 862-869. (d) Williams, D. E.; Rietman, J. A.; Maier, J. M.; Tan, R.; Greytak, A. B.; Smith, M. D.; Krause, J. A.; Shustova, N. B., Energy Transfer on Demand: Photoswitch-Directed Behavior of Metal–Porphyrin Frameworks. *J. Am. Chem. Soc.* **2014**, *136*, 11886-11889.
- (16) Huang, C. B.; Xu, L.; Zhu, J. L.; Wang, Y. X.; Sun, B.; Li, X.; Yang, H. B. Real-Time Monitoring the Dynamics of Coordination-Driven Self-Assembly by Fluorescence-Resonance Energy Transfer. *J. Am. Chem. Soc.* **2017**, *139*, 9459-9462.
- (17) (a) Li, Z.; Kishi, N.; Hasegawa, K.; Akita, M.; Yoshizawa, M. Highly Fluorescent M_2L_4 Molecular Capsules with Anthracene Shells. *Chem. Commun.* **2011**, *47*, 8605-8607. (b) Yan, X.; Wei, P.; Liu, Y.; Wang, M.; Chen, C.; Zhao, J.; Li, G.; Saha, M. L.; Zhou, Z.; An, Z.; Li, X.; Stang, P. J. Endo- and Exo-Functionalized Tetraphenylethylene $M_{12}L_{24}$ Nanospheres: Fluorescence Emission inside a Confined Space. *J. Am. Chem. Soc.* **2019**, *141*, 9673-9679.
- (18) (a) Yan, X.; Cook, T. R.; Wang, P.; Huang, F.; Stang, P. J., Highly emissive platinum(II) metallacages. *Nat. Chem.* **2015**, *7*, 342-348. (b) Yan, X.; Wang, M.; Cook, T. R.; Zhang, M.; Saha, M. L.; Zhou, Z.; Li, X.; Huang, F.; Stang, P. J., Light-Emitting Superstructures

- with Anion Effect: Coordination-Driven Self-Assembly of Pure Tetraphenylethylene Metallacycles and Metallacages. *J. Am. Chem. Soc.* **2016**, *138*, 4580-4588. (c) Yu, G.; Zhang, M.; Saha, M. L.; Mao, Z.; Chen, J.; Yao, Y.; Zhou, Z.; Liu, Y.; Gao, C.; Huang, F.; Chen, X.; Stang, P. J. Antitumor Activity of a Unique Polymer That Incorporates a Fluorescent Self-Assembled Metallacycle. *J. Am. Chem. Soc.* **2017**, *139*, 15940-15949. (d) Lu, C.; Zhang, M.; Tang, D.; Yan, X.; Zhang, Z.; Zhou, Z.; Song, B.; Wang, H.; Li, X.; Yin, S.; Sepehrpour, H.; Stang, P. J., Fluorescent Metallacage-Core Supramolecular Polymer Gel Formed by Orthogonal Metal Coordination and Host-Guest Interactions. *J. Am. Chem. Soc.* **2018**, *140*, 7674-7680.
- (19) (a) Shustova, N. B.; McCarthy, B. D.; Dinca, M. Turn-On Fluorescence in Tetraphenylethylene-Based Metal-Organic Frameworks: An Alternative to Aggregation-Induced Emission. *J. Am. Chem. Soc.* **2011**, *133*, 20126-20129. (b) Zhang, M.; Feng, G.; Song, Z.; Zhou, Y. P.; Chao, H. Y.; Yuan, D.; Tan, T. T.; Guo, Z.; Hu, Z.; Tang, B. Z.; Liu, B.; Zhao, D. Two-Dimensional Metal-Organic Framework with Wide Channels and Responsive Turn-On Fluorescence for the Chemical Sensing of Volatile Organic Compounds. *J. Am. Chem. Soc.* **2014**, *136*, 7241-7244. (c) Zhao, J.; Yang, D.; Zhao, Y.; Yang, X.-J.; Wang, Y.-Y.; Wu, B. Anion-Coordination-Induced Turn-On Fluorescence of an Oligourea-Functionalized Tetraphenylethene in a Wide Concentration Range. *Angew. Chem. Int. Ed.* **2014**, *53*, 6632-6636. (d) Sinha, N.; Stegemann, L.; Tan, T. T. Y.; Doltsinis, N. L.; Strassert, C. A.; Hahn, F. E. Turn-On Fluorescence in Tetra-NHC Ligands by Rigidification through Metal Complexation: An Alternative to Aggregation-Induced Emission. *Angew. Chem. Int. Ed.* **2017**, *56*, 2785-2789. (e) Yin, G. Q.; Wang, H.; Wang, X. Q.; Song, B.; Chen, L. J.; Wang, L.; Hao, X. Q.; Yang, H. B.; Li, X. Self-Assembly of Emissive Supramolecular Rosettes with Increasing Complexity Using Multitopic

- Terpyridine Ligands. *Nat. Commun.* **2018**, *9*, 567. (f) Liu, N.; Lin, T.; Wu, M.; Luo, H. K.; Huang, S. L.; Hor, T. S. A. Suite of Organoplatinum(II) Triangular Metallaprism: Aggregation-Induced Emission and Coordination Sequence Induced Emission Tuning. *J. Am. Chem. Soc.* **2019**, *141*, 9448-9452. (g) Li, Y.; An, Y. Y.; Fan, J. Z.; Liu, X. X.; Li, X.; Hahn, F. E.; Wang, Y. Y.; Han, Y. F. Strategy for the Construction of Diverse Poly-NHC-Derived Assemblies and Their Photoinduced Transformations. *Angew. Chem. Int. Ed.* **2019**, *58*, doi: 10.1002/anie.201912322.
- (20) (a) Hong, Y.; Lam, J. W. Y.; Tang, B. Z. Aggregation-Induced Emission. *Chem. Soc. Rev.* **2011**, *40*, 5361-5388. (b) Mei, J.; Leung, N. L.; Kwok, R. T.; Lam, J. W.; Tang, B. Z. Aggregation-Induced Emission: Together We Shine, United We Soar! *Chem. Rev.* **2015**, *115*, 11718-11940.
- (21) (a) Yan, X.; Wang, H.; Hauke, C. E.; Cook, T. R.; Wang, M.; Saha, M. L.; Zhou, Z.; Zhang, M.; Li, X.; Huang, F.; Stang, P. J. A Suite of Tetraphenylethylene-Based Discrete Organoplatinum(II) Metallacycles: Controllable Structure and Stoichiometry, Aggregation-Induced Emission, and Nitroaromatics Sensing. *J. Am. Chem. Soc.* **2015**, *137*, 15276-15286. (b) Zhang, M.; Saha, M. L.; Wang, M.; Zhou, Z.; Song, B.; Lu, C.; Yan, X.; Li, X.; Huang, F.; Yin, S.; Stang, P. J. Multicomponent Platinum(II) Cages with Tunable Emission and Amino Acid Sensing. *J. Am. Chem. Soc.* **2017**, *139*, 5067-5074.
- (22) (a) Zhang, M.; Yin, S.; Zhang, J.; Zhou, Z.; Saha, M. L.; Lu, C.; Stang, P. J. Metallacycle-cored supramolecular assemblies with tunable fluorescence including white-light emission. *Proc. Natl. Acad. Sci. USA* **2017**, *114*, 3044-3049. (b) Sun, Y.; Yao, Y.; Wang, H.; Fu, W.; Chen, C.; Saha, M. L.; Zhang, M.; Datta, S.; Zhou, Z.; Yu, H.; Li, X.; Stang, P. J., Self-Assembly of Metallacages into Multidimensional Suprastructures with Tunable Emissions. *J. Am. Chem. Soc.* **2018**, *140*, 12819-12828.

- (23) (a) Zhang, Z.; Zhao, Z.; Hou, Y.; Wang, H.; Li, X.; He, G.; Zhang, M. Aqueous Platinum(II)-Cage-Based Light-Harvesting System for Photocatalytic Cross-Coupling Hydrogen Evolution Reaction. *Angew. Chem. Int. Ed.* **2019**, *58*, 8862-8866. (b) Acharyya, K.; Bhattacharyya, S.; Sepehrpour, H.; Chakraborty, S.; Lu, S.; Shi, B.; Li, X.; Mukherjee, P. S.; Stang, P. J. Self-Assembled Fluorescent Pt(II) Metallacycles as Artificial Light-Harvesting Systems. *J. Am. Chem. Soc.* **2019**, *141*, 14565-14569.
- (24) Sagara, Y.; Yamane, S.; Mitani, M.; Weder, C.; Kato, T. Mechanoresponsive Luminescent Molecular Assemblies: An Emerging Class of Materials. *Adv. Mater.* **2016**, *28*, 1073-1095.
- (25) (a) Yuan, H.; Wang, K.; Yang, K.; Liu, B.; Zou, B. Luminescence Properties of Compressed Tetraphenylethene: The Role of Intermolecular Interactions. *J. Phys. Chem. Lett.* **2014**, *5*, 2968-2973. (b) Ma, Z.; Wang, Z.; Meng, X.; Ma, Z.; Xu, Z.; Ma, Y.; Jia, X. A Mechanochromic Single Crystal: Turning Two Color Changes into a Tricolored Switch. *Angew. Chem. Int. Ed.* **2016**, *55*, 519-522. (c) Qiu, Z.; Zhao, W.; Cao, M.; Wang, Y.; Lam, J. W. Y.; Zhang, Z.; Chen, X.; Tang, B. Z. Dynamic Visualization of Stress/Strain Distribution and Fatigue Crack Propagation by an Organic Mechanoresponsive AIE Luminogen. *Adv. Mater.* **2018**, *30*, e1803924.
- (26) (a) Zhang, Q.; Su, J.; Feng, D.; Wei, Z.; Zou, X.; Zhou, H. C. Piezofluorochromic Metal–Organic Framework: A Microscissor Lift. *J. Am. Chem. Soc.* **2015**, *137*, 10064-10067. (b) Chen, C. X.; Wei, Z. W.; Fan, Y. N.; Su, P. Y.; Ai, Y. Y.; Qiu, Q. F.; Wu, K.; Yin, S. Y.; Pan, M.; Su, C. Y. Visualization of Anisotropic and Stepwise Piezofluorochromism in an MOF Single Crystal. *Chem* **2018**, *4*, 2658-2669.
- (27) Liu, Y.; Zeng, Q.; Zou, B.; Liu, Y.; Xu, B.; Tian, W. Piezochromic Luminescence of Donor-Acceptor Cocrystals: Distinct Responses to Anisotropic Grinding and Isotropic Compression. *Angew. Chem. Int. Ed.* **2018**, *57*, 15670-15674.

- (28) Dewaele, A.; Loubeyre, P.; Occelli, F.; Marie, O.; Mezouar, M. Toroidal Diamond Anvil Cell for Detailed Measurements under Extreme Static Pressures. *Nat. Commun.* **2018**, *9*, 2913.
- (29) (a) Tang, J. H.; Sun, Y.; Gong, Z. L.; Li, Z. Y.; Zhou, Z.; Wang, H.; Li, X.; Saha, M. L.; Zhong, Y. W.; Stang, P. J. Temperature-Responsive Fluorescent Organoplatinum(II) Metallacycles. *J. Am. Chem. Soc.* **2018**, *140*, 7723-7729. (b) Sun, Z.-B.; Liu, J.-K.; Yuan, D.-F.; Zhao, Z.-H.; Zhu, X.-Z.; Liu, D.-H.; Peng, Q.; Zhao, C.-H., 2,2'-Diamino-6,6'-diboryl-1,1'-binaphthyl: A Versatile Building Block for Temperature-Dependent Dual Fluorescence and Switchable Circularly Polarized Luminescence. *Angew. Chem. Int. Ed.* **2019**, *58*, 4840-4846.
- (30) The emission response of cages **4a** and **4b** as solid powders to the temperature were also collected and shown in Figure S62.

TOC Graphic:

